Reports in Mechanical Engineering
Vol. 6, No. 1, 2025, pp. 112-126
ISSN: 2683-5894, DOI: https://doi.org/10.31181/rme489

Nonlinear Multimode Vibration Attenuation of Cantilever Beams using Tuned Passive Shunt Circuits

Khaled Kadri, Samir Emam*, Khaled Al-Souqi
Department of Mechanical Engineering, American University of Sharjah, PO Box 26666, Sharjah, United Arab Emirates

Article Info

Article history:

Received August 15, 2025
Revised September 17, 2025
Accepted October 10, 2025

Keywords:

Vibration Control,
Cantilever Beams,
Geometric Nonlinearity,
Shunted Circuit,
Optimization

ABSTRACT

This paper investigates the vibration attenuation of the multimode linear and nonlinear responses of cantilever beams using tuned passive shunt circuits. The vibration control is achieved via the optimization of the R-L circuit parameters for the maximum vibration attenuation over the frequency domain of interest using a Particle Swarm Optimization (PSO) algorithm of MATLAB. A mathematical model is developed for the coupled multimode response of a cantilever beam attached with a piezoelectric (PZT) shunt circuit. The geometrical and inertia nonlinearities of the cantilever beam are taken into consideration. The optimization technique is based on minimizing the area under the frequency-response plot as an objective function over the desired frequency domain. The effect of the PZT location and size is examined. The tuned shunt circuit parameters are found to significantly reduce the multi-mode nonlinear vibration of the beam. The tuned electrical natural frequency of the absorber is found to shift away from the beam's natural frequency as the excitation force is increased. Additionally, adding a nonlinear inductor to the circuit is found to be insignificant and hence tuning the linear R-L circuit is an efficient treatment for the linear and nonlinear vibration of cantilever beams.

Corresponding Author:

Samir Emam
Department of Mechanical Engineering, American University of Sharjah, PO Box 26666, Sharjah, United Arab Emirates
Email: semam@aus.edu

1. Introduction

Reducing the weight of a structure has been a common goal for most engineering applications to increase efficiency and effectiveness. Nevertheless, light structures are prone to vibration that may cause constraints in performance (Inman D.J. & Singh, 2022). Vibrations can have a negative impact on systems ranging from reduced accuracy and efficiency, noise pollution, and even mechanical failure due to fatigue. Therefore, it is important to take into account the effects of vibration when it comes to designing engineering machines and structures (Thomson, 1996). There are three main categories regarding vibration attenuation: active, semi-active, and passive. The active methods require a powered electrical component and a control system to obtain the desired performance for vibration reduction. The need for an external power source causes issues in the design, simplicity, and practicality of the application. Therefore, active vibration control achieves vibration control over a broader range of frequencies. On the other hand, mitigating vibrations using passive techniques is difficult at low frequencies (Fuller et al., 1990). The traditional method of passively minimizing the effects of vibrations on a structure is by using a mass-spring-damper system that is typically known as a tuned-mass damper (TMD). However, this technique adds undesirable weight to the system where the goal of the design of some applications is to reduce the weight of the part. In addition, the mass-spring-damper system is sensitive to detuning, which would be a complicated process to fix (Yang et al., 2022). Piezoelectric materials connected to shunted circuits have been used as vibrational absorbers as an alternative to the TMDs. Hybrid methods combine aspects from both active and passive control methods. Hybrid methods use passive techniques with the support of active components (Baz, 2019). Nonlinear shunted damping is energy-efficient due to its passive nature, making it preferable in low-power or energy-constrained environments (e.g., satellites, remote infrastructure). Active

control, while effective, demands continuous power, limiting its use in such scenarios. Nonlinear shunted damping offers moderate performance with minimal complexity, suitable for applications where simplicity and reliability are prioritized. Active control provides superior performance but at the cost of increased complexity, cost, and maintenance, making it better suited for high-stakes or high-precision applications. Nonlinear shunted damping is more robust in harsh environments (e.g., extreme temperatures, radiation) due to its passive nature. Active control systems may require protective measures for sensors and actuators in such conditions. Nonlinear shunted damping is easier to scale for small, distributed systems (e.g., multiple piezoelectric patches on a structure). Active control is more scalable for large systems (e.g., entire buildings) but requires significant infrastructure. In real-world examples, nonlinear shunted damping is used in aerospace for vibration control in satellite panels, where piezoelectric patches with nonlinear circuits reduce vibrations without power consumption. Also applied in automotive engine mounts to dampen variable-frequency vibrations. Active control employed in modern skyscrapers (e.g., active mass dampers in the Burj Khalifa) to counteract wind-induced vibrations and in advanced aircraft for active flutter control, ensuring stability at high speeds. Forward (Forward, 1979) proposed converting strain energy into electrical energy by use of piezoelectric transducers coupled to electrical components and modify the physical parameters of the system to suppress vibration. The control applications for piezoelectric materials include active, passive, and hybrid techniques. Active piezoelectric damping systems provide an effective and adaptable technique for improving the dynamic responsiveness, stability, and overall performance of engineering systems. By incorporating piezoelectric components into structures and applying precise electrical signals, the piezoelectric component could be used as a transducer (Bailey & Hubbard Jr, 1985; Hashemi et al., 2022; Li et al., 2023). The passive control technique includes a piezoelectric patch attached to the main structure which is then connected to an electrical circuit in order to achieve the required vibration attenuation. The concept was first introduced by Hagood and von Flotow (Hagood & Von Flotow, 1991) where the piezoelectric transducer is shunted to a resistor that functions as a viscoelastic damper. The value of the resistor was tuned based on the natural frequency of the base structure. The limitation of this technique was that damping a low-frequency resonance requires a low electrical frequency, which requires large inductors. However, different circuits have been used to achieve the desired vibration reduction (Yamada, 2017). In addition, some shunt electrical circuits can tackle the issues of multimode vibration and nonlinear vibration. A closed magnetic core inductor made of high-permeability material increases inductance for better performance in resonant circuits, while multi-layer piezoelectric elements enhance equivalent capacitance, reducing the need for high inductance (Thomas et al., 2011). The use of a negative capacitor for nonlinear vibration control of subsonic thin plate has been studied (Wang et al., 2024). An improved LRLC shunted circuit with an additional capacitor introduces dual resonances for increased robustness and performance (Berardengo et al., 2020). The nonlinear piezoelectric tuned vibration absorber (NPTVA) utilizes a ferrite-based closed magnetic circuit and nonlinear principles to effectively attenuate vibrations in nonlinear systems(Lossouarn et al., 2017). Finite element and reduced-order models facilitate vibration damping analysis and tuning techniques without physical experiments, enabling optimal placement of piezoelectric patches and multimodal vibration reduction (da Silva et al., 2012; Deü et al., 2014; Nguyen & Pietrzko, 2006; Thomas et al., 2009). Basic resistor (R) and resonant shunt (RL) circuits struggle to mitigate nonlinearities caused by geometric, material, and boundary condition factors (Lossouarn et al., 2017; Plumbridge et al., 2003). Active methods like linear quadratic regulators (LQR) controllers and negative capacitance systems provide real-time responses and enhanced vibration damping but require external power and amplifiers, limiting their focus in this proposal (Hashemi & Jang, 2022). In contrast, the nonlinear piezoelectric tuned vibration absorber (NPTVA) offers a fully passive solution. Utilizing ferrite-based closed magnetic circuits, the NPTVA achieves high inductance and effectively attenuates vibrations in nonlinear structures by leveraging the nonlinear similarity principle. While experimental and numerical results confirm the NPTVA's efficacy, its performance diminishes when excitation forces exceed a certain threshold (Lossouarn et al., 2017). Furthermore, the idea of nonlinear energy sinks using piezoelectric material has been studied (Dekemele et al., 2024; Silva et al., 2018; Zhou & Hu, 2023). While traditional methods focus on single-mode reduction, addressing multiple modes is critical for improved efficiency, particularly in nonlinear systems. Hollkamp (Hollkamp, 1994) introduced the use of a single piezoelectric element with additional LRC circuit branches to suppress multiple structural modes, deriving and experimentally validating a multimodal transfer function on a cantilevered beam. Wu (Wu, 1998) proposed a multi-mode shunting method using additional circuit blocks (C-L in parallel) in series with single-mode shunt circuits. This approach simplified circuit design and demonstrated effective two- and three-mode damping, though multiple PZT patches are necessary in low-strain regions. Behrens et al. (Behrens et al., 2003) presented a "current flowing" shunt controller, which efficiently dampens multiple modes with fewer circuit elements. The method, validated on a beam and plate structure, achieved equivalent performance to previous schemes while reducing component complexity. Recent advances in alleviating vibrations of offshore wind turbines (OWTs) using active tuned mass dampers (TMDs) are investigated by Han et al. (Han et al., 2026). The active TMD is regulated using a linear quadratic regulator controller. Dynamic vibration absorber arrays

(DVAAs) showed an effective vibration attenuation ability within the intended range of their tuned parameters. However, its performance tends to degrade significantly at large mistuning conditions. Zhang et al. (Zhang et al., 2026) proposed an optimization approach that introduces intentional deviation to the natural frequencies of the DVAs to enhance the robustness of their performance. The use of the piezoelectric shunted circuits for vibration attention has been well established in the literature. However, many of the cases in literature concerned with lumped-parameter systems or single-mode modelling of linear distributed-parameter systems. There is a lack in studies based on multimode nonlinear attenuation. The objective of this paper is to develop a mathematical model and an optimization technique for the attenuation of the multi-mode nonlinear vibration of a cantilever beam using passive shunted circuits. The beam's geometric and inertia nonlinearities are taken into consideration. The vibration attenuation is studied around the first two vibration modes. Frequency response plots are used to assess the response of the beam with and without the vibration absorber at different frequencies. Two different types of circuits are used: a linear RL circuit with a resistor and an inductor and a nonlinear RL circuit with a resistor and a negative inductor. The negative inductor works based on the magnetic saturation of ferrite inductors. The particle swarm optimisation (PSO) function of MATLAB is used to find the optimum tuned circuit parameters for the maximum vibration reduction. Two objective functions are used for the optimization: the first aims at minimizing the area under the frequency response plot and the second aims at minimizing the maximum peak of the frequency response curve. Furthermore, the significance of the location and length of the piezoelectric patches are studied. Moreover, a comparison between using linear circuits to attenuate the nonlinear responses and using a nonlinear circuit to attenuate the nonlinear responses is discussed.

2. Problem Formulation

In this section, we develop a mathematical model for the multi-mode electromechanical behaviour of a cantilever beam attached to a shunt circuit. The model accounts for the inertia and geometric nonlinearities of the structure (Arafat et al., 1998). The circuit consists of two parts: an RL circuit in series and another RL circuit incorporating a negative inductor, similar to the approach proposed by Lossouarn et al. (Lossouarn et al., 2018) to address system nonlinearities. To attenuate the vibrations across multiple modes, a current-blocking technique is used. The number of circuit branches corresponds to the number of modes targeted for attenuation. Tuning the electrical components is achieved using a Particle Swarm Optimization (PSO) algorithm in MATLAB. The nonlinear lateral vibration of a cantilever beam accounting for the geometric and inertia nonlinearities is governed by the following equations (Arafat et al., 1998):

$$\rho A\ddot{v} + EIv'''' + \frac{\rho A}{2}\left\{ v' \int_l^x \frac{\partial^2}{\partial t^2}\left[\int_0^x (v')^2\, dx\right] dx\right\}' + EI[v'(v'v'')']' = F\cos(\Omega t) \tag{1}$$

$$v(0,t) = 0, v'(0,t) = 0,\ v''(l,t) = 0,\ v'''(l,t) = 0 \tag{2}$$

Where $v(x,t)$ is the amplitude of the lateral vibration; the beam's material and geometrical properties E, I, ρA, and l are, respectively, the beam's elastic modulus, area moment of inertia, mass per unit length, and length; F and Ω are the amplitude and frequency of the applied harmonic force; x is the spatial coordinate, and t is time. The dot and dash denote the derivatives with respect to time and length, respectively. The properties of the beam are given in Table 1.

Table 1: Geometric and Material Characteristics of the Cantilever Beam.

Parameter	Value
Length (m)	0.3
Width (m)	0.02
Thickness (m)	0.001
Area (mm2)	2.0×10^{-15}
Elastic Modulus (GPa)	210
Density (kg/m^3)	7800
Second Moment of Inertia (m^4)	1.667×10^{-12}

The standard solution for the linear vibration problem and the derivation of the discretized equations using the Galerkin's method are outlined in the Appendix. Lossouarn et al. (Lossouarn et al., 2018) and Shami et al. (Zein A Shami et al., 2022; Shami et al., 2023; Zein Alabidin Shami et al., 2022) presented the coupled electromechanical equations for lumped systems with PZT shunts. We extend their approach to model continuous systems and present the coupled governing equations as follows:

$$\ddot{q}_n + 2\zeta_n\omega_n\dot{q}_n + \omega_n^2 q_n + \sum_{i,j,k}^{N} b_{ijkn} q_i q_j q_k + e_n V = f_n \cos(\Omega t), n = 1,2,\ldots,N \quad (3a)$$

$$C^{\epsilon} V - Q - \sum_{i}^{N} e_i q_i = 0 \quad (3b)$$

$$L\ddot{Q} + R\dot{Q} + V = 0 \quad (3c)$$

Where e_n is the piezoelectric coupling coefficient, C^{ϵ} is the capacitance of the piezoelectric patch, and V and Q are the voltage and electrical charges respectively. The capacitance $C^{\epsilon}$is defined as:

$$C^{\epsilon} = \frac{\epsilon^T \epsilon^0 l_p w_p}{t_P} \quad (4)$$

Where ϵ^T and $\epsilon^0$are the permittivity and piezoelectric coefficients, l_p,w_p, and t_p are the piezoelectric length, width and thickness. Götz (Götz et al., 2014) showed that the electromechanical coupling coefficient e_n is given as

$$e_n = \frac{1}{\rho A}\int_0^1 2E_p\epsilon^0 w_p \frac{(t+t_p)}{2}\,\varphi_n''(\bar{x})\Delta H d\bar{x} \quad (5)$$

Where $\Delta H = H(\bar{x}-a) - H(\bar{x}-b)$ is the Heaviside function, E_p is the piezoelectric elastic modulus. The material considered in this study is soft PZT-P (Zr.Ti)O_3 C-82 with properties given in Table 2. Equations (11a) to (11c) can be manipulated and reduced to the following:

$$\ddot{q}_n + 2\zeta_n\omega_n\dot{q}_n + \omega_n^2 q_n + \frac{e_n}{C^{\epsilon}}\left(\sum_{i}^{N} e_i\, q_i + Q\right) + \sum_{i,j,k}^{N} b_{ijkn} q_i q_j q_k = f_n \sin(\Omega t), n = 1,2,\ldots,N \quad (6)$$

$$\ddot{Q} + 2\,\zeta_e\omega_e\dot{Q} + \omega_e^2 Q + \frac{1}{LC^{\epsilon}}\sum_{i}^{N} e_i q_i = 0 \quad (7)$$

Where ω_e is an electrical natural frequency and ζ_e is damping ratio defined as

$$\omega_e = \frac{1}{\sqrt{LC^{\epsilon}}}, \qquad \zeta_e = \frac{1}{2}R\sqrt{\frac{C^{\epsilon}}{L}} \quad (8)$$

Table 2: Piezoelectric Patch Properties.

Parameter	Value
Width (mm)	20
Thickness (mm)	0.5
Elastic Modulus (GPa)	62.9
Permittivity	3650
Piezoelectric Coefficient (C/N)	266×10^{-12}

3. Results and Discussion

3.1 Effect of the Piezoelectric Patch Parameters

This section presents the results of the mathematical model using MATLAB simulation. The frequency response plots are used as a measure to illustrate the behaviour of the cantilever beam under various excitation conditions and circuit parameters. Figure 1 shows the three patch placements considered in this study: (a) on the beam's root, (b) middle, and (c) tip. The parameters a and b identify the patch positions measured from the beam's root, as shown in the figure. It can be noticed that the patch location affects in the first place the electromechanical coupling coefficient, as given in Eq. (5). The piezoelectric patch is connected to a circuit whose resistor, R, and inductor, L, are calculated using different criteria such as the equal-peak method. The values of electromechanical coupling coefficient e_n for the first three modes for the three patch locations are presented in Table 3. As the table shows, the coupling coefficient

of the first mode is maximum when the patch is attached at the beam's root. Other modes have their maximum coupling coefficient far from the root. Nevertheless, the first mode contributes the most to the response and hence is expected that the root location of the patch will be the choice to increase the coupling. Figure 1 shows the frequency response plot (FRP) around the first mode of the uncontrolled and controlled system. The equal-peak method is used to tune the circuit parameters for the maximum vibration attenuation for the three patch locations. As the figure shows, attaching the PZT patch to the beam's root resulted in the best performance regarding the vibration suppression. Putting the PZT patch on the beam's tip resulted in the least vibration suppression.

Table 3: Electromechanical coupling coefficients for different patch location and size.

PZT Patch Location (m)	e_1	e_2	e_3
Root: $a = 0, b = 0.1$	3.230×10^{-3}	6.43×10^{-3}	6.21×10^{-3}
Middle: $a = 0.1, b = 0.2$	1.475×10^{-3}	1.72×10^{-2}	1.94×10^{-3}
Tip: $a = 0.2, b = 0.3$	2.465×10^{-4}	6.64×10^{-3}	3.29×10^{-2}

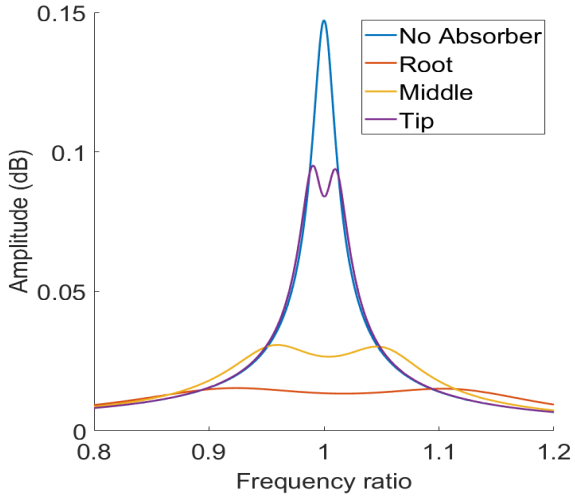

Figure 1: The Frequency-Response Plots of the Beam's Tip Point.

Moreover, the effect of the piezoelectric patch length as shown in Fig. 3 is studied. The corresponding patch capacitance and coupling coefficient is shown in Table 4. As the PZT patch length increases, its capacitance and electromechanical coupling coefficient increase. Fig. 3 shows the frequency response plots of the beam's response with different patch lengths. It can be noticed that changing the patch length does not significantly affect the vibration suppression. This is because the PZT patch is less effective far from the beam's root as outlined earlier. Therefore, using a patch length of 5-10 cm for the beam used in this study, which is about 16-33 % of the beam's length, is efficient.

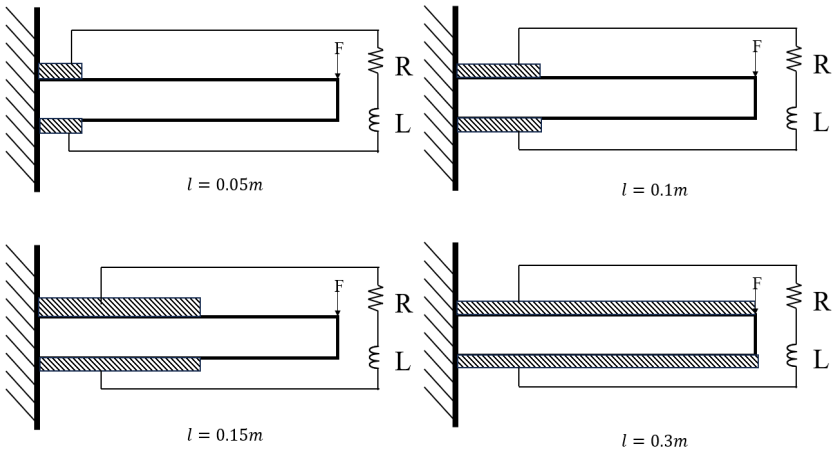

Figure 2: A Cantilever Beam with PZT Patches of Different Lengths.

Table 4: Piezoelectric Patch Capacitance and Electromechanical Coupling Coefficient for Different PZT Lengths.

PZT Patch Length (m)	C^{ϵ}	e_1
$l = 0.05$	6.4727×10^{-6}	1.893×10^{-3}
$l = 0.1$	12.945×10^{-6}	3.230×10^{-3}
$l = 0.15$	19.418×10^{-6}	4.243×10^{-3}
$l = 0.3$	38.836×10^{-6}	5.022×10^{-3}

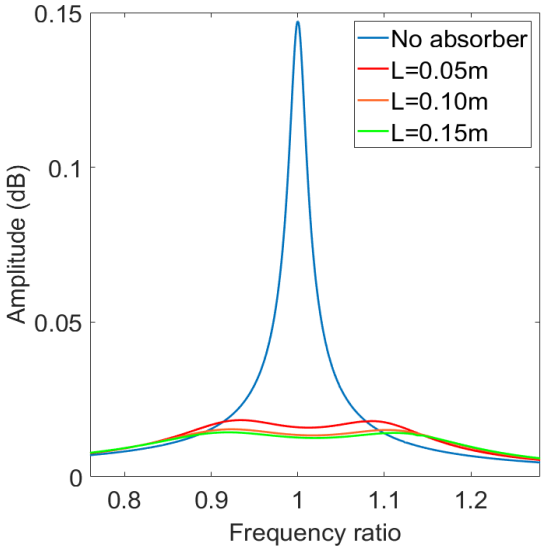

Figure 3: Frequency-Response Plots for the Beam's Tip Point Without and with PZT Patches of Different Lengths.

3.2 Linear Response using a Single-Mode Approximation

The linear vibration of the cantilever beam considering only the first mode contribution is governed by Eq. (14) after neglecting the nonlinear term as setting the number of modes equal to unity. The result is

$$\ddot{q}_1 + 2\zeta_1\omega_1\dot{q}_1 + \left(\omega_1^2 + \frac{e_1^2}{C^{\epsilon}}\right)q_1 + \frac{e_1}{C^{\epsilon}}Q = f_1\sin(\Omega t) \tag{16a}$$

$$\ddot{Q} + 2\,\zeta_e\omega_e\dot{Q} + \omega_e^2 Q + \frac{1}{LC^{\epsilon}}e_1 q_1 = 0 \tag{16b}$$

The beam is excited by a point force at its tip. Three tuning methods are considered to identify the optimum circuit parameters: the resistance R and inductance L: the well-known equal-peak tunning (Den Hartog, 1985; Habib et al., 2015), the minimum area under the frequency-response plot, and the minimum peak. The particle swarm optimization (PSO) technique in MATLAB is used to find the optimum tuning circuit parameters for a given objective function, as shown in Table 5. For each method, the frequency ratio that is the ratio of the absorber's natural frequency and the beam's natural frequency is calculated. As the table shows, for the linear vibration of the beam using a linear circuit, the three methods generate similar results for the optimum frequency ratio, circuit parameters, and the percent of the vibration reduction. The equal-peak method can be used for a two-degree-of-freedom system and hence other methods need to be used for the multi-mode approximation. Figure 4 shows a comparison of the frequency response plot for the beam's response using different tuning methods. The results benchmark the performance of the optimization tunning techniques to that of the conventional method that is the equal-peak method. The computational time of the minimum-area optimization method was significantly larger than that of the minimum-peak. Therefore, the minimum-peak method is used for the results to come. The time response of the beam's tip point with and without the absorber is shown in Fig. 5. As the figure shows, the shunt circuit drastically reduces the vibration amplitude.

Table 5: Optimum Linear Circuit Parameters Using Different Tuning Techniques.

Tuning Method	L (H)	R (Ω)	Frequency ratio	Reduction (%)
Equal Peaks	840.4	2408	0.972	88.5
Minimum Area	837.5	1834	0.970	89.7

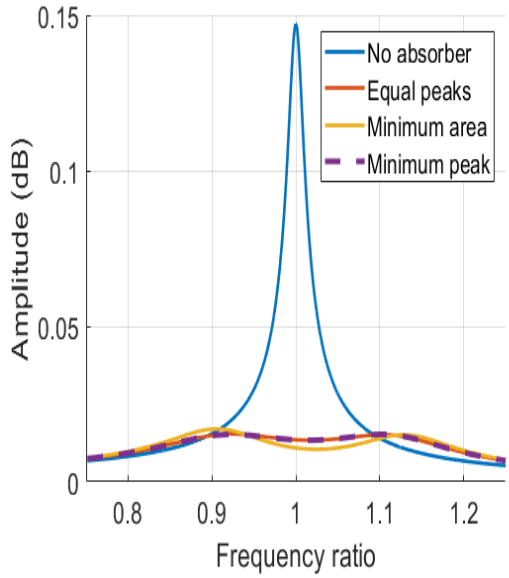

Figure 4: The Frequency-Response Plots for the Linear Vibration of the Beam's Tip Point Using a Single Mode and a Linear Shunt Circuit at F=0.001N.

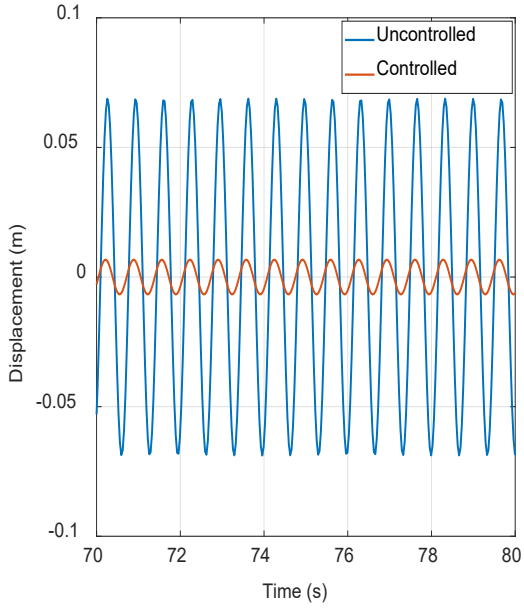

Figure 5: Time Response of the Beam's Tip with and Without the Absorber.

3.3 Linear Response using a Multi-Mode Approximation

The multi-mode approximation of the linear response of the beam is governed by Eqs. (14) after eliminating the nonlinear geometric nonlinearity term and letting N be more than 1. Figure 6 shows the frequency-response plots of the beam at a forcing amplitude of 0.001 N using a single mode and two modes in the discretization over the frequency domain of the first two modes. The frequency ratio ω_{ratio} refers to the excitation frequency divided by the first natural frequency. As the figure shows, the first peak is identical for the single and multiple-mode approximations. Apparently, single-mode approximation captures only the contribution of the first mode and hence it does not detect the higher modes. By employing the current blocking method on the circuit, it is applicable to suppress the vibration around multiple modes. Minimizing the area under the frequency-response plot over the frequency domain of interest results in the optimum tuning parameters, as shown in Table 6. Using the tuned circuit parameters, the frequency-response plot of the controlled beam is shown in Fig. 8.

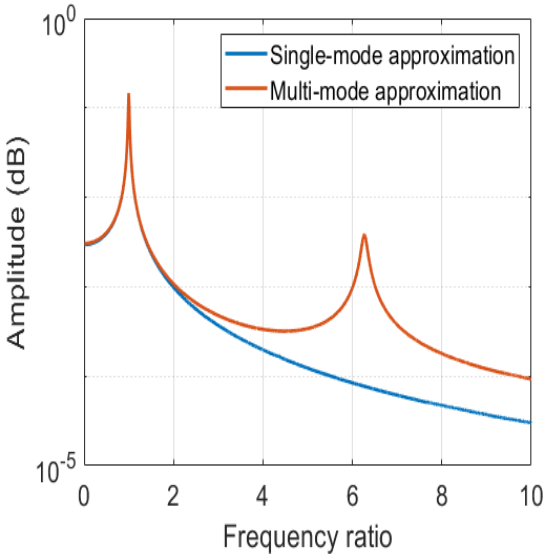

Figure 6: Frequency Response Plots using a Single Mode and a Multiple Mode Discretization.

Table 6: Tuned Electric Circuit Parameters for Multi-Mode Response.

Mode	L (H)	R (Ω)	Frequency ratio	Reduction (%)
First Mode	835.1	2421.0	0.968	89.0
Second Mode	22.3	93.2	0.992	64.9

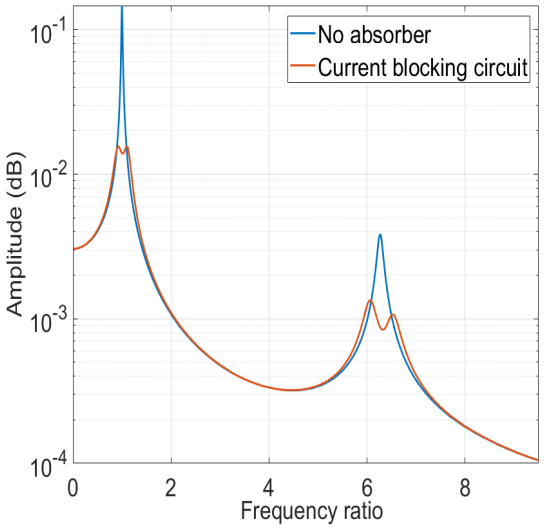

Figure 7: Multiple Mode Linear Cantilever Beam with Linear Shunted Circuit FRP.

3.4 Nonlinear Response using a Multi-Mode Approximation

Here, we consider the full nonlinear model using multi-mode approximation, as given in Eqs. (14). Considering nonlinearities gives a more realistic response of the beam compared to the linear model. Figure 9 shows the frequency-response plot for the linear and the nonlinear models. The nonlinear model shows bending to the right for the frequency response, which reflects the hardening nonlinearity that the system has. The frequency-response plot for the nonlinear beam shows also a region with multiple solutions and discontinuity that allows the jump phenomenon to happen upon the forward and backward frequency sweep. Figure 9 shows the frequency-response plots for different forcing amplitudes. As the figure shows, as the force amplitude increases, as the force increases, the bending behaviour of the beam increases. The response changes qualitatively as the frequency window of the multiple solutions widens, and quantitatively by increasing the response amplitude.

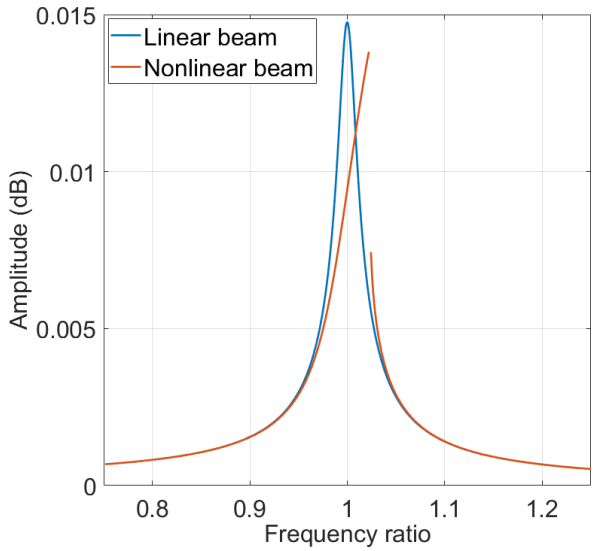

Figure 8: Frequency-Response Plots for the Linear and the Nonlinear Beam F=0.001N.

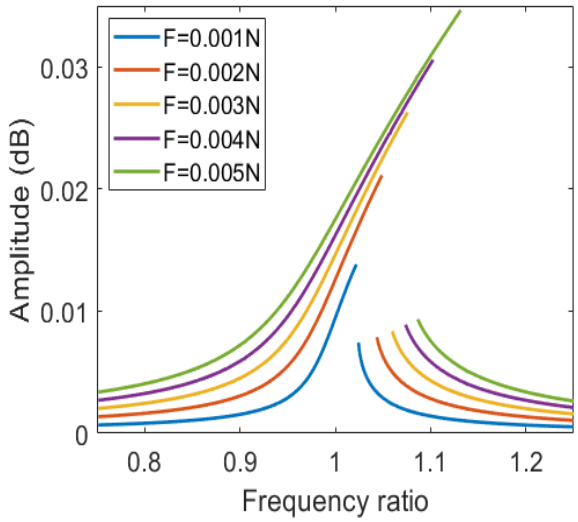

Figure 9: Frequency-Response Plots for the Nonlinear Beam with Various Force Amplitudes.

The literature presents many articles that employ a nonlinear component to the electrical circuit absorber to attenuate the nonlinear vibration of the structure. Here, a negative inductor is considered. The negative inductor works on the principle of magnetic saturation. With a linear inductor, as the current increases the inductance increases. On the other hand, the inductance of the nonlinear inductor increases with the increase of current until it reaches the point of magnetic saturation. Beyond the point of magnetic saturation, the increases of the current leads to a decrease of inductance as shown in Fig. 10. The modified equation of motion for the nonlinear beam with a nonlinear RL circuit is exactly as Eqs. (14) where the linear inductance L is replaced with the negative nonlinear inductance L^* defined as

$$L^* = L\left(1 - \alpha\, \dot{Q}^2\right) \tag{17}$$

Where α is a design parameter of the inductor that is estimated via the PSO optimization. Figure 11 shows the variation of the inductance of a nonlinear inductor with the current according to (Burrascano et al., 2018). The frequency-response plots for the beam's response using a linear and a nonlinear shunt circuit at a forcing amplitude of 0.001 N and 0.025N, respectively, is shown in Figs. 12 and 13. As it is evident from the figure, the nonlinear inductance is insignificant regarding the vibration suppression compared with the linear inductance. Therefore, for this case, the linear shunt circuit is sufficient. The optimum tuning parameters of the circuit and hence the absorber's

frequency for the linear and nonlinear circuits at two forcing amplitudes are given in Table 7. It can be noticed that the tuned frequency ratio shifts to the left as the forcing amplitude increases and becomes significantly away from the unity.

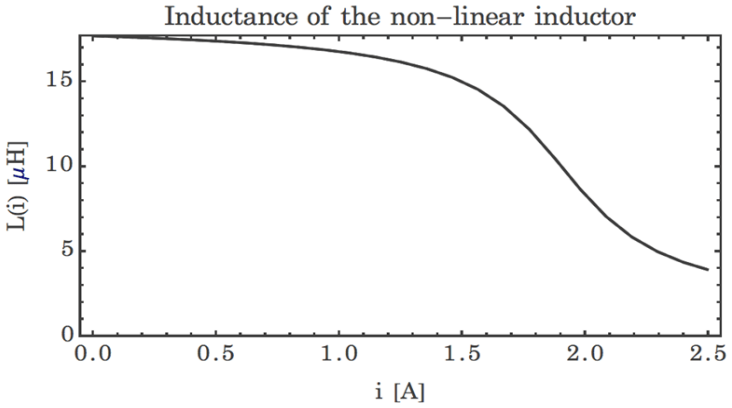

Figure 10: Variation of the Inductance of a Nonlinear Inductor with the Current (Den Hartog, 1985).

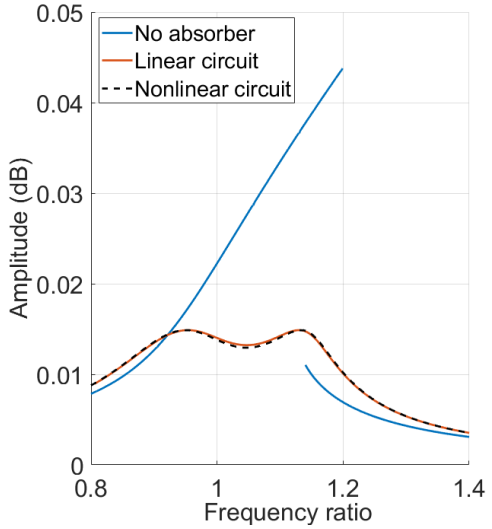

Figure 11: The Frequency-Response Plot of the First Mode Using a Linear and a Nonlinear Shunted Circuit at a Forcing of 0.001 N.

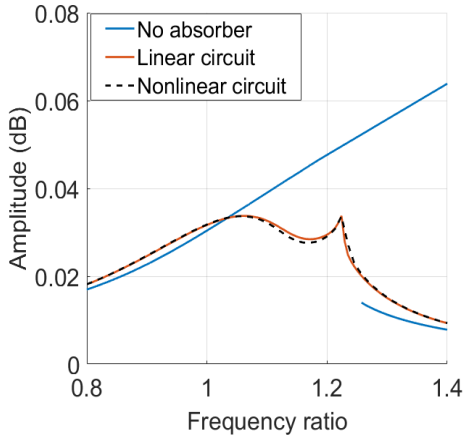

Figure 12: The Frequency-Response Plot Around the First Mode Using a Linear and a Nonlinear Shunted Circuit at a Forcing of 0.025 N.

Table 7: Tuned Circuit Parameters, Frequency Ratio, and Vibration Attenuation with Varying Force Amplitude.

Type of the Circuit	Force (N)	L(H)	R(Ω)	α	Tuned Frequency Ratio	Attenuation (%)
Linear Circuit	0.01	797.5	2314.4	—	0.946	66.1
Nonlinear Circuit	0.01	798.9	2260.3	1.46	0.947	66.1
Linear Circuit	0.025	657.7	1877.8	—	0.859	53.2
Nonlinear Circuit	0.025	659.8	1834.4	1.66	0.861	53.2

Finally, the multi-mode vibration attenuation of cantilever beams with relatively large amplitude where the geometric nonlinearity becomes significant is presented. The current blocking approach is used in order to tune the circuit to attenuate multiple modes. The optimum circuit parameters using the PSO optimization approach, the tuned frequency ratio of the absorber, and the percent attenuation reduction around the first two modes are presented in Table 8. Figure 13 shows the frequency response of the multi-mode response of the geometrically nonlinear cantilever beam using a tuned linear shunt circuit.

Table 8: Tuned Circuit Parameters and Frequency Ratio Using the Current Blocking Approach.

Mode	Tuned Circuit Parameters		Tuned Frequency Ratio	Reduction (%)
	L (H)	R (Ω)		
First	792.6	2260.4	0.943	72.1
Second	22.6	128.3	0.998	69.9

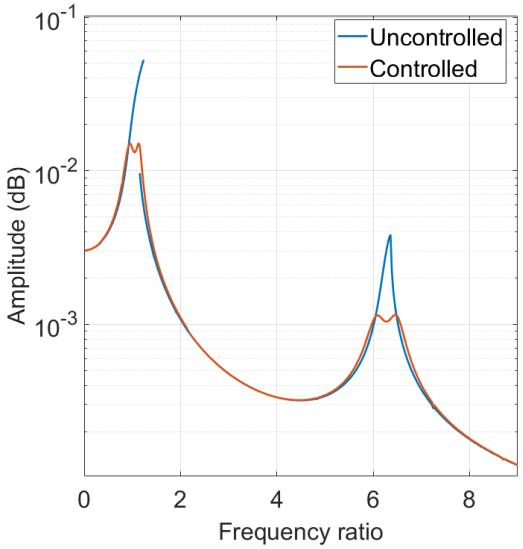

Figure 13: The Frequency Response Plots for the Multi-Mode Nonlinear Response of the Beam with and Without the Shunt Circuit.

4. Conclusion

The linear and nonlinear multimode vibration attenuation of cantilever beams using a tuned shunt circuit was investigated. A mathematical model of the beam considering the inertia and geometric nonlinearities coupled with a piezoelectric patch and RL circuit was derived. A discretized model for the governing equation is obtained using Galerkin's method. A current blocking method was used to passively deal with the multimode mode response. A Particle Swarm Optimization (PSO) algorithm of MATLAB was used to find the optimal parameters of the electrical circuit using the minimum area under the frequency-response plot as an objective function. The model was validated versus well-known tuning methods such as the equal-peak method. A parametric study was performed to assess the effectiveness of the PZT patch and circuit parameters on the resulting vibration of the beam. The optimization algorithm was successful to identify the tuned parameters, and a significant reduction of the vibration ranging from 50% to 89% was reported. The results show that a linear RL circuit with proper tuning is sufficient to suppress the beam's vibration and adding a nonlinearity to the inductor does not show a significant improvement in the absorber's performance. With the presence of the beam's geometric nonlinearity and as the excitation force increases, it was found that the tuned electrical frequency becomes a head of the beam's natural frequency and a frequency ratio

significantly less than one.

Nomenclature

Variable	Description
a, b	Piezoelectric Patch Location
a_{ijkn}	Inertia Nonlinearity Term
b_{ijkn}	Geometric Nonlinearity Term
C^{ε}	Capacitance of the Piezoelectric Patch
E	Modulus of Elasticity
e_n	Electromechanical Coupling Coefficient
E_p	Elastic Modulus if Piezoelectric Material
F	Amplitude of the Harmonic Force
f_n	Modal Force
I	Second Moment of Inertia
l	Beam Length
L	Inductance
L^*	Nonlinear Inductance
l_p	Piezoelectric Patch Length
N	Number of Modes
Q	Electric Charge
q_i	Generalized Coordinates
R	Resistance
t	Time
t_p	Piezoelectric Patch Thickness
v	Lateral Vibration
V	Voltage
V_n	Frequency Coefficients
w_p	Piezoelectric Patch Width
x	Special Coordinate Along the Length of the Beam
$\bar{x}$	Nondimensional Spatial Coordinate
ρA	Mass Per Unit Length
α	Nonlinear Inductor Coefficient
Ω	Force Frequency
ω_n	Natural Frequency
φ_n	Mode Shape
ζ_n	Damping Ratio
ϵ^0	Piezoelectric Charge Coefficient
ϵ^t	Permittivity

Funding Statement

The authors declare that this work received no funding.

Conflict of Interest Statement

The authors declare that there is no conflict of interest to declare.

References

Arafat, H. N., Nayfeh, A. H., & Chin, C.-M. (1998). Nonlinear nonplanar dynamics of parametrically excited cantilever beams. *Nonlinear Dynamics*, *15*(1), 31-61. https://doi.org/10.1023/A:1008218009139

Bailey, T., & Hubbard Jr, J. E. (1985). Distributed piezoelectric-polymer active vibration control of a cantilever beam. *Journal of Guidance, Control, and Dynamics*, *8*(5), 605-611. https://doi.org/10.2514/3.20029

Baz, A. M. (2019). *Active and passive vibration damping*. John Wiley & Sons. https://books.google.com/books?hl=en&lr=&id=nR1-

DwAAQBAJ&oi=fnd&pg=PA17&dq=Active+and+Passive+Vibration+Damping&ots=05V0PY5C61&sig=uHL9HsJ8L5kTZVCabfNzKvCNicg

Behrens, S., Moheimani, S. R., & Fleming, A. (2003). Multiple mode current flowing passive piezoelectric shunt controller. *Journal of sound and vibration*, *266*(5), 929-942. https://doi.org/10.1016/S0022-460X(02)01380-9

Berardengo, M., Høgsberg, J., Manzoni, S., Vanali, M., Brandt, A., & Godi, T. (2020). LRLC-shunted piezoelectric vibration absorber. *Journal of sound and vibration*, *474*, 115268. https://doi.org/10.1016/j.jsv.2020.115268

Burrascano, P., Di Capua, G., Femia, N., Laureti, S., & Ricci, M. (2018). Pulse compression for ferrite inductors modeling in moderate saturation. In *2018 15th International Conference on Synthesis, Modeling, Analysis and Simulation Methods and Applications to Circuit Design (SMACD)* (pp. 229-232). IEEE. https://doi.org/10.1109/SMACD.2018.8434903.

da Silva, L. P., Deü, J.-F., Larbi, W., Trindade, M. A., & Métiers, P. (2012). An efficient finite element approach for reduction of structural vibration and acoustic radiation by passive shunted piezoelectric systems. In *Proceedings of the 10th World Congress on Computational Mechanics, WCCM* (pp. 8-13). https://doi.org/10.5151/meceng-wccm2012-18811

Dekemele, K., Giraud-Audine, C., & Thomas, O. (2024). A piezoelectric nonlinear energy sink shunt for vibration damping. *Mechanical Systems and Signal Processing*, *220*, 111615. https://doi.org/10.1016/j.ymssp.2024.111615

Den Hartog, J. P. (1985). *Mechanical vibrations*. Courier Corporation. https://books.google.com/books?hl=en&lr=&id=IshIAwAAQBAJ&oi=fnd&pg=PP1&dq=Mechanical+Vibrations&ots=E8fXqwu7Dl&sig=sCJw-4pvEHzfNfSv5VTII26ZS2A

Deü, J.-F., Larbi, W., Ohayon, R., & Sampaio, R. (2014). Piezoelectric shunt vibration damping of structural-acoustic systems: finite element formulation and reduced-order model. *Journal of Vibration and Acoustics*, *136*(3), 031007. https://doi.org/10.1115/1.4027133

Forward, R. L. (1979). Electronic damping of vibrations in optical structures. *Applied Optics*, *18*(5), 690-697. https://doi.org/10.1364/AO.18.000690

Fuller, C., Gibbs, G., & Silcox, R. (1990). Simultaneous active control of flexural and extensional waves in beams. *Journal of Intelligent Material Systems and Structures*, *1*(2), 235-247. https://doi.org/10.1177/1045389X9000100206

Götz, B., Platz, R., & Melz, T. (2014). Effect of uncertain boundary conditions and uncertain axial loading on lateral vibration attenuation of a beam with shunted piezoelectric transducers. In *Proceedings of ISMA2014 including USD2014 International Conference on Uncertainty in Structural Dynamics* (pp. 4495-4508). https://past.isma-isaac.be/downloads/isma2014/papers/isma2014_0161.pdf

Habib, G., Detroux, T., Viguié, R., & Kerschen, G. (2015). Nonlinear generalization of Den Hartog′ s equal-peak method. *Mechanical Systems and Signal Processing*, *52*, 17-28. https://doi.org/10.1016/j.ymssp.2014.08.009

Hagood, N. W., & Von Flotow, A. (1991). Damping of structural vibrations with piezoelectric materials and passive electrical networks. *Journal of sound and vibration*, *146*(2), 243-268. https://doi.org/10.1016/0022-460X(91)90762-9

Han, D., Wang, W., Li, X., & Su, X. (2026). Vibration Suppression of Offshore Wind Turbine Under Multi-Hazards by Active Tuned Mass Damper. *Journal of Offshore Mechanics and Arctic Engineering*, *148*(1), 012001. https://doi.org/10.1115/1.4068684

Hashemi, A., & Jang, J. (2022). Smart Active Vibration Control System of a Wind Turbine Blade Using Piezoelectric Material. In *Dynamics of Civil Structures, Volume 2: Proceedings of the 40th IMAC, A Conference and Exposition on Structural Dynamics 2022* (pp. 1-15). Springer. https://doi.org/10.1007/978-3-031-05449-5_1

Hashemi, A., Jang, J., & Hosseini-Hashemi, S. (2022). Smart active vibration control system of a rotary structure using piezoelectric materials. *Sensors*, *22*(15), 5691. https://doi.org/10.3390/s22155691

Hollkamp, J. J. (1994). Multimodal passive vibration suppression with piezoelectric materials and resonant shunts. *Journal of Intelligent Material Systems and Structures*, *5*(1), 49-57. https://doi.org/10.1177/1045389X9400500106

Inman D.J., & Singh, R. C. (2022). *Engineering Vibration* (5th ed.). Boston: Pearson. https://api.pageplace.de/preview/DT0400.9780273785217_A24571595/preview-9780273785217_A24571595.pdf

Li, C., Shen, L., Shao, J., & Fang, J. (2023). Simulation and experiment of active vibration control based on flexible piezoelectric MFC composed of PZT and PI layer. *Polymers*, *15*(8), 1819. https://doi.org/10.3390/polym15081819

Lossouarn, B., Aucejo, M., Deü, J.-F., & Multon, B. (2017). Design of inductors with high inductance values for resonant piezoelectric damping. *Sensors and Actuators A: Physical*, *259*, 68-76. https://doi.org/10.1016/j.sna.2017.03.030

Lossouarn, B., Deü, J.-F., & Kerschen, G. (2018). A fully passive nonlinear piezoelectric vibration absorber. *Philosophical transactions of the royal society A: mathematical, physical and engineering sciences*, *376*(2127), 20170142. https://doi.org/10.1098/rsta.2017.0142

Nguyen, C., & Pietrzko, S. (2006). FE analysis of a PZT-actuated adaptive beam with vibration damping using a parallel R–L shunt circuit. *Finite elements in analysis and design*, *42*(14-15), 1231-1239. https://doi.org/10.1016/j.finel.2006.06.003

Plumbridge, W., Matela, R. J., & Westwater, A. (2003). *Structural integrity and reliability in electronics: enhancing performance in a lead-free environment*. Springer. https://doi.org/10.1007/1-4020-2611-0

Shami, Z. A., Giraud-Audine, C., & Thomas, O. (2022). A nonlinear piezoelectric shunt absorber with a 2: 1 internal resonance: Theory. *Mechanical Systems and Signal Processing*, *170*, 108768. https://doi.org/10.1016/j.ymssp.2021.108768

Shami, Z. A., Giraud-Audine, C., & Thomas, O. (2023). Saturation correction for a piezoelectric shunt absorber based on 2: 1 internal resonance using a cubic nonlinearity. *Smart Materials and Structures*, *32*(5), 055024. https://doi.org/10.1088/1361-665X/acc994

Shami, Z. A., Shen, Y., Giraud-Audine, C., Touzé, C., & Thomas, O. (2022). Nonlinear dynamics of coupled oscillators in 1: 2 internal resonance: effects of the non-resonant quadratic terms and recovery of the saturation effect. *Meccanica*, *57*(11), 2701-2731. https://doi.org/10.1007/s11012-022-01566-w

Silva, T. M., Clementino, M. A., De Marqui Jr, C., & Erturk, A. (2018). An experimentally validated piezoelectric nonlinear energy sink for wideband vibration attenuation. *Journal of sound and vibration*, *437*, 68-78. https://doi.org/10.1016/j.jsv.2018.08.038

Thomas, O., Deü, J. F., & Ducarne, J. (2009). Vibrations of an elastic structure with shunted piezoelectric patches: efficient finite element formulation and electromechanical coupling coefficients. *International Journal for Numerical Methods in Engineering*, *80*(2), 235-268. https://doi.org/10.1002/nme.2632

Thomas, O., Ducarne, J., & Deü, J.-F. (2011). Performance of piezoelectric shunts for vibration reduction. *Smart Materials and Structures*, *21*(1), 015008. https://doi.org/10.1088/0964-1726/21/1/015008

Thomson, W. (1996). *Theory of Vibration with Applications*. CRC Press. https://doi.org/10.1201/9780203718841

Wang, C., Yao, G., & Liu, M. (2024). Passive vibration control of subsonic thin plate via nonlinear capacitance and negative capacitance coupled piezoelectric shunt damping. *Thin-Walled Structures*, *198*, 111656. https://doi.org/10.1016/j.tws.2024.111656

Wu, S.-Y. (1998). Method for multiple mode piezoelectric shunting with single PZT transducer for vibration control. *Journal of Intelligent Material Systems and Structures*, *9*(12), 991-998. https://doi.org/10.1177/1045389X9800901204

Yamada, K. (2017). Complete passive vibration suppression using multi-layered piezoelectric element, inductor, and resistor. *Journal of sound and vibration*, *387*, 16-35. https://doi.org/10.1016/j.jsv.2016.10.009

Yang, F., Sedaghati, R., & Esmailzadeh, E. (2022). Vibration suppression of structures using tuned mass damper technology: A state-of-the-art review. *Journal of Vibration and Control*, *28*(7-8), 812-836. https://doi.org/10.1177/1077546320984305

Zhang, K., Wang, S., Wu, J., Zheng, C., & Bi, C. (2026). Robust optimization of dynamic vibration absorber array for vibration attenuation of mistuned bladed disk. *Journal of Vibration and Acoustics*, *148*(1), 011002. https://doi.org/10.1115/1.4069367

Zhou, K., & Hu, Z. (2023). Vibration suppression on the composite laminated plates subjected to aerodynamic and harmonic excitations based on the nonlinear piezoelectric shunt damping. *Applied Mathematical Modelling*, *121*, 134-165. https://doi.org/10.1016/j.apm.2023.04.026

Appendix

Following the standard procedure, the linear-free vibration mode shapes and natural frequencies are defined as follows:

$$\varphi(\bar{x}) = \sin(V_i\bar{x}) - \sinh(V_i\bar{x}) - \frac{\sinh(V_i) + \sin(V_i)}{\cosh(V_i) + \cos(V_i)} \left(\cos(V_i\bar{x}) - \cosh\left(V_i\bar{x}\right)\right) \tag{A1}$$

$$\omega_i = \sqrt{\frac{EI}{\rho A l^4}} V_i^2 \tag{A2}$$

Where $\bar{x}$ is a nondimensional spatial coordinate defined as $\bar{x} = x/l$ and V_n are constant frequency coefficients defined as

$$\cos V_n \cosh V_n + 1 = 0 \tag{A3}$$

The orthogonality conditions are defined as follows:

$$\int_0^1 \varphi_i(\bar{x})\varphi_j(\bar{x})\, dx = \begin{cases} 1, i = j \\ 0, i \neq j \end{cases}$$

$$\int_0^1 \varphi_i(\bar{x})''''\varphi_j(\bar{x})\, dx = \begin{cases} V_n^4, i = j \\ 0, i \neq j \end{cases} \tag{A4}$$

The governing partial-differential equation, Eq. (1), is discretised into a set of ordinary-differential equations using Galerkin's method. Therefore, we let the displacement $v(\bar{x}, t)$ be discretized using N modes as follows:

$$v(\bar{x}, t) = \sum_{i=1}^{N} \varphi_i(\bar{x})\, q_i(t) \tag{A5}$$

Where φ_i and q_i are, respectively, the vibration mode shapes and generalized coordinates. Substituting Eq. (A5) into Eq. (1), multiplying the resulting equation by φ_n, integrating over the domain, noting the orthogonality conditions, and adding modal damping, we obtain

$$\ddot{q}_n + 2\zeta_n\omega_n\dot{q}_n + \omega_n^2 q_n + \sum_{i,j,k}^{N} a_{ijkn}\, q_i\, \frac{\partial^2}{\partial t^2}(q_j q_k) + \sum_{i,j,k}^{N} b_{ijkn}\, q_i q_j q_k = f_n \cos\Omega t, n = 1, 2, \dots, N \tag{A6}$$

Where,

$$a_{ijkn} = \frac{1}{2L^2}\int_0^1 \left\{\sum_i^N \varphi_n'(\bar{x}) \int_1^{\bar{x}} \left[\int_0^{\bar{x}} \sum_j^N \sum_k^N \varphi_j'(\bar{x})\, \varphi_k'(\bar{x}) d\bar{x}\right] d\bar{x}\right\}' \varphi_n(\bar{x})\, d\bar{x} \tag{A7}$$

$$b_{ijkn} = \frac{EI}{\rho A l^6} \int_0^1 \left[\sum_i^N \varphi_i'(\bar{x}) \left(\sum_j^N \sum_k^N \varphi_j'(\bar{x})\varphi_k''(\bar{x})\right)'\right]' \varphi_n(\bar{x}) \tag{A8}$$

$$f_n = \frac{1}{\rho A}\int_0^1 F(\bar{x})\, \varphi_n(\bar{x})\; d\bar{x} \tag{A9}$$

Equation (A6) represents N-nonlinearly coupled ordinary-differential equations that can be numerically integrated for the coordinates qs. The discretized equation accounts for the inertia nonlinearity, the first nonlinear term, and the geometric nonlinearity, the second nonlinear term. Both nonlinearities are of cubic type. The inertia nonlinearity was found to be negligible for the case considered in this paper. As a result, the discretized equation becomes.

$$\ddot{q}_n + 2\zeta_n\omega_n\dot{q}_n + \omega_n^2 q_n + \sum_{i,j,k}^{N} b_{ijkn} q_i q_j q_k \; = f_n \cos(\Omega t)\,, \qquad n = 1,2, \dots, N \tag{A10}$$